Changes of the Membrane Lipid Organization Characterized by Means of a New Cholesterol-Pyrene Probe

Laurent Le Guyader,* Christophe Le Roux,† Serge Mazères,* Hafida Gaspard-Iloughmane,† Heinz Gornitzka,† Claire Millot,* Christophe Mingotaud,‡ and André Lopez*

*Institut de Pharmacologie et de Biologie Structurale, Toulouse, France; and †Laboratoire d'Hétérochimie Fondamentale et Appliquée, and ‡Laboratoire des Interactions Moléculaires et Réactivité Chimique et Photochimique, Université Paul Sabatier, Toulouse, France

ABSTRACT We synthesized 3β-hydroxy-pregn-5-ene-21-(1-methylpyrenyl)-20-methylidene (Py-met-chol), consisting of cholesterol steroid rings connected to a pyrene group via a linker without polar atoms. This compound has interesting spectroscopic properties when probing membranes: 1), The pyrene has hypochromic properties resulting from probe self-association processes in membranes. Using liposomes of various lipid compositions, we determined the association constants of the probe (K): $K_{DOPC} \gg K_{POPC} \gg K_{DMPC} > K_{DMPC/15\ mol\ \%\ Chol} > K_{DMPC/30\ mol\ \%\ Chol}$. This indicates a better probe solvation in saturated than in unsaturated lipids, and this effect is enhanced as the cholesterol concentration increases. 2), The pyrene fluorophore is characterized by monomer (I_1–I_5) and excimer (I_E) emission bands. In model membranes, I_1/I_3 and I_E/I_3 ratios revealed a correlation between the polarity of the lipid core of the membrane and the amount of cholesterol. 3), Using this probe, we monitored the first steps of the signaling pathway of the mouse δ-opioid receptor, a G-protein-coupled receptor. The thickness of the membrane around this receptor is known to change after agonist binding. Fluorescence spectra of living Chinese hamster ovary cells overexpressing mouse δ-opioid receptor specifically revealed the agonist binding. These results indicate that Py-met-chol may be useful for screening ligands of this family of receptors.

INTRODUCTION

The plasma membrane is a complicated mixture of lipids and proteins, organized into various specialized microdomains (1), which differ in their composition, their physical properties, and, consequently, their biological functions (2,3). These distinct microdomains cannot be directly identified in living cells by noninvasive approaches. However, numerous studies of detergent-resistant membrane fractions and of reconstituted model membranes of comparable lipid compositions (4,5) indicate that some lipids have the propensity to associate with each other and to promote lateral segregation (6). This is the case for mixtures of cholesterol, sphingolipids, and saturated glycerophospholipids, which generate a liquid-ordered (lo) fluid phase (2). This phase is characterized by more tightly packed hydrophobic moieties, lipids having a weaker translational diffusion and no rotational diffusion (2,3,7,8), and a thicker membrane than the liquid-disordered (ld) phase composed of unsaturated glycerophospholipids with the same acyl chain lengths (9). Such lipid effects may occur in plasma membrane; indeed, some G-protein-coupled receptors (GPCRs) change the thickness of the membrane after ligand binding, as reported by Salamon et al. for the mouse δ-opioid receptor (mDOR) in reconstituted membranes (10).

All of the biophysical approaches for quantifying these general properties use model membranes with simple lipid mixtures, whereas investigations on in vivo cell membranes require indirect methods. Various fluorescent membrane probes, for example, the 1,6-diphenyl-1,3,5-hexatriene derivatives (11) or prodan/laurdan probes (12), have been used to determine membrane structure and lipid molecular organization. Another family of probes based on pyrene allows the investigation of the lateral distribution and the dynamics of membrane compounds (13). Indeed, the monomer (M) and the excimer (E) species have different fluorescence signals (I_M and I_E, respectively) (13), and the ratio of fluorescence intensities (I_E/I_M) is directly related to the probe distribution in the lipid membrane network (14). Moreover, pyrene is an effective spectroscopic sensor of the polarity of the membrane's hydrophobic core (15): the monomer fluorescence spectrum consists of five emission bands, where I_1 is a function of the polarity of the probe's surroundings and I_3 is mainly proportional to the probe's concentration. Thus, the ratio I_1/I_3 is of particular interest for membrane studies, because an increase in the mole fraction of cholesterol is correlated with a decrease of the membrane's permeability to water (16). Since the polarity within a lipid membrane is mostly determined by the number of internal water molecules present (17), the pyrene probe should report the cholesterol-induced lo phase with respect to the ld phase.

In a previous study (18) of a cholesterol-pyrene-based probe (1-pyrenemethyl-(3β)-3-hydroxy-22,23-bisnor-5-cholenate (Py-ester-chol)), we identified several interesting properties

Submitted May 15, 2007, and accepted for publication August 14, 2007.

Address reprint requests to André Lopez, Institut de Pharmacologie et de Biologie Structurale, UMR 5089, 205 route de Narbonne, 31077 Toulouse cedex, France. Tel.: 33(0)-561-175-945; Fax: 33(0)-561-175-994; E-mail: andre.lopez@ipbs.fr.

Editor: Thomas J. McIntosh.

0006-3495/07/12/4462/12 $2.00

doi: 10.1529/biophysj.107.112821

of this probe family, but its low miscibility in lipid bilayers made labeling living cell plasma membranes impossible. This low miscibility was attributed to the polar atoms present in the linker between the cholesterol moiety and the pyrene moiety. To avoid this problem, we synthesized 3β-hydroxy-pregn-5-ene-21-(1-methylpyrenyl)-20-methylidene (Py-met-chol), a new probe designed without polar atoms in the linker. We first characterized its membrane behavior, and then used absorbance measurements to study its lateral distribution in model membranes. The fluorescence experiments, carried out with model membranes of various compositions, allowed us to characterize changes in the core polarity and lipid organization, since both of these features are correlated with changes in the membrane thickness. Finally, we used the probe to label living cell plasma membranes and their fluorescence properties to detect the first steps of a cell signaling pathway, triggered by the thickness change associated with mDOR binding its agonist (10).

MATERIALS AND METHODS

Organic synthesis of Py-met-chol

The scheme and the detailed description of the chemical synthesis, the infrared, NMR ^{1}H and ^{13}C characteristics, the analytical characterizations, and the RX molecular structure of tert-butyldimethylsilyl-(Py-met-chol) are described in the Supplementary Material.

Lipids and other reagents

Cholesterol, 1,2-dimyristoyl-*sn*-glycero-3-phosphocholine (DMPC), 1-palmitoyl-2-oleoyl-*sn*-glycero-3-phosphocholine (POPC), and 1,2-dioleoyl-*sn*-glycero-3-phosphocholine (DOPC) were purchased from Sigma (St Louis, MO), and 1,2-dipalmitoyl-*sn*-glycero-3-phosphocholine (DPPC) was purchased from Avanti Polar Lipids (Alabaster, AL). The purity of phospholipids and sterols was confirmed by thin-layer chromatography on silica-gel (Merck, Darmstadt, Germany) using chloroform/methanol/water (65:25:4, v/v) as the elution solvent. The detections were performed with the Dittmer's reagent for phosphorus compounds (19) and then heated to detect sterols. Lipids, dissolved in chloroform/methanol (9:1, v/v) were stored at 4°C before use. The concentrations of phospholipid solutions were determined by a classical phosphate assay and by a colorimetric method (20) for cholesterol and Py-met-chol. A gravimetric approach using a Sartorius (Goettingen, Germany) super microbalance (10^{-7} g) was also used. Diprenorphin and Deltorphin II were purchased from Sigma. Water was purified through a Milli-Q system (Millipore, Bedford, MA).

Preparation of lipid vesicles

Liposomes were prepared by mixing appropriate volumes of the stock solutions of phospholipids, cholesterol, or Py-met-chol (mole fractions were calculated according to the total quantity of lipids in a given suspension). Solvent was evaporated under a nitrogen stream and samples were desiccated under vacuum for 2 h (1 Torr). The dried lipid samples were hydrated in MOPS buffer (10 mM 3-morpholino-propanesulfonic acid, 100 mM NaCl, and 0.02% w/v NaN_3, pH 7.4) and heated to 60°C for 20 min (this temperature is higher than the gel-to-liquid transition temperature (T_m)). We immediately vortexed the sample for 4 min to allow the formation of multilamellar vesicles (MLVs). For absorbance and fluorescence experiments, MLVs (at final concentrations of 0.1–1 mM) were sonicated for 10 min at a temperature above the T_m using a VibraCell sonicator (Sonics & Materials, Newtown, CT) with a titanium-plated tip delivering 12.5 W. The samples, constituted of small unilamellar vesicle suspensions, were immediately centrifuged for 25 min at 20,000 $\times$ *g* (5408R centrifuge, Eppendorf, Hamburg, Germany) to remove any titanium particles. Small unilamellar vesicle suspensions were stored for 36 h to allow vesicle fusion. The sizes of relaxed large unilamellar vesicles (LUVs) were measured by dynamic light scattering using a Dynapro device (Wyatt Technology, Santa Barbara, CA). The LUVs in this study had a mean radius of 77 $\pm$ 6 nm.

Differential scanning calorimetry

MLVs (at a final concentration of 30 mM) were subjected to three cycles of freezing and heating to 60°C for 10 min for MLV homogenization. The samples were stored at 4°C for at least 24 h and then loaded into the sample cell of the calorimeter; ~45 mg of each MLV suspension was sealed into a stainless steel high-pressure capsule and scanned at rates of 600, 300, 150, 105, 60, 45, 30, and 15°C/h from 5°C to 60°C and from 60°C to 5°C on a Pyris-1 calorimeter (Perkin-Elmer, Norwalk, CT) (the reference was an empty capsule). The amount of probe was maintained below its maximum solubility in all cases. For all samples, we analyzed the scans to assess the maximum temperature and the enthalpy of the gel-to-liquid phase transition for each scanning rate. By extrapolation to 0°C/h, we obtained the exact melting enthalpy.

Absorption spectrometry

Absorption spectra were measured from 500 to 280 nm in a 1-cm path length quartz cuvette using a Uvikon 923 spectrophotometer (Kontron Instruments, Milan, Italy) equipped with a thermostated cuvette holder at 30 $\pm$ 0.1°C (Fisher Bioblock Scientific, Illkirch, France). We used air as the reference to calibrate a zero baseline. The molar absorption coefficients of the probe ε_{meas} were calculated from the absorbance at 345 nm of each liposome suspension. This corresponds to the lowest energy-absorption band of the monosubstituted pyrene. To eliminate the effect of liposome light scattering at this wavelength, we used a homemade program calculating the contribution of the turbidity ($T(\lambda)$) to the absorbance spectrum of each sample. This program is based on an equation (Eq. 1) modified from that described previously (21):

$$T(\lambda) = A \times \frac{1}{\lambda^{B}} + C, \quad (1)$$

where λ is the wavelength and A, B, and C are the parameters that have to be fitted. Using nonlinear regression, we determined the parameter values from experimental measurements of absorbance at 290 nm and from 385 nm to 500 nm in a given sample. Thus, the turbidity value at 345 nm was calculated and allowed accurate measurement of the probe absorbance. We used the Beer-Lambert law and these absorbance values to determine ε_{meas} values for all samples.

Fluorescence spectrometry

Emission spectra were recorded on a QuantaMaster-4 spectrofluorimeter (Photon Technology International, Birmingham, NJ) monitored by FeliX32 software. The excitation wavelength (bandwidth 5 nm) was set to 330 nm to avoid the Raman peak of water. The fluorescence emission (bandwidth 2 nm) was measured from 365 to 600 nm in 0.5-nm increments. The signal integration time was set to 100 ms for vesicle suspensions and to 200 ms for cell suspensions. Fluorescence spectra were recorded in 1-cm quartz cuvettes thermostated at 37 $\pm$ 0.1°C (Fisher Bioblock Scientific) for LUVs and labeled Chinese hamster ovary (CHO) cells. I_1, I_3, and I_E were measured at 376, 388, and 475 nm, respectively.

Determination of the maximum solubility of Py-met-chol in liposomes

We prepared POPC liposomes at a final concentration of 0.1 mM with a series of mole fractions of the probe (0.15–0.35 mol %). All probe molecules not incorporated into liposomes formed aggregates in the buffer with a specific spectral response. These aggregates were eliminated by centrifugation for 25 min at 20,000 × *g* (5408R, Eppendorf). We then measured (at 20°C) the absorbance of each suspension at 345 nm as a function of the mole fraction of the probe. The Py-met-chol mole fraction for which the absorbance reached a plateau was taken as the maximum solubility.

Isodesmic model

Calculations were performed using the isodesmic model (18) described in the Appendix. This model accounts for changes in the absorption (hypochromism) of the probe's pyrene moiety due to a self-association process in membranes where the association constants, K, are equivalent for each association step. The pyrene probe absorbs light as a monomer (ε_{mono}) and as n-mers, where the two pyrene molecules at the ends absorb light as half-stacked mers (ε_{ext}) and n-2 pyrene molecules inside an n-mer absorb light as fully stacked mers (ε_{int}). For a given liposome suspension, the overall absorption (ε_{calc}) corresponds to the sum of these three contributions weighted by their respective mole fractions. Parameter fitting (K, ε_{mono}, ε_{ext}, ε_{int}) is performed by minimizing the sum of the squares of weighted residuals ($1/\varepsilon^2_{meas}$) between ε_{meas} and ε_{calc} to account for the increased experimental error as the probe concentration decreases.

Labeling mixture preparation

Methyl-β-cyclodextrin (MβCD, Sigma) was dissolved in water (683 mg in 7 mL) and heated to 70°C under agitation. To obtain a 1:75 molar ratio (Py-met-chol/MβCD), 50 μL of a solution of Py-met-chol in dimethylformamide (138 mM) was added slowly. This solution was sterilized through a 0.22-μm-pore filter and stored for up to several weeks at 4°C. The incubation medium consisted of 1 mL of this solution diluted (1:30, v/v) in phosphate-buffered saline (PBS) (Gibco-BRL, Cergy-Pontoise, France) and warmed to 37°C. The final dimethylformamide concentration was <0.05%. The final concentration of MβCD was 2.5 mM.

Cell culture and in vivo plasma membrane labeling

We used CHO cells stably transfected (CHO-δ) with the gene for the mouse δ-opioid 7-transmembrane receptor (mDOR), which was produced at a rate of 10 ± 1 pmol receptor/mg protein. CHO wild-type cells (CHO-wt) were used as controls. Cells were grown in culture flasks in supplemented HAM-F12 nutrient mixture (10% fetal calf serum, 2 mM sodium glutamate, 50 μg/mL penicillin and streptomycin) at 37°C under a 5% CO_2 atmosphere. Geneticin (0.8%, v/v) was added for selection of transfected cells. The cells were plated on coverslips, washed twice with 1 mL of PBS without calcium at 37°C, and incubated with 1 mL of labeling mixture for 2 min at 37°C. The inoculum was removed and cells were washed six times with PBS without calcium and then suspended in HEPES buffer (20 mM HEPES, 118 mM choline chloride, 10 mM glucose, 3 mM $MgSO_4$, 1.5 mM $CaCl_2$, pH 7.4). Four minutes later, we added an mDOR agonist (Deltorphin II) or antagonist (Diprenorphin) to a final concentration of 1 μM to the CHO or CHO-δ cell suspensions. All products were purchased from Gibco-BRL, Invitrogen.

Fluorescence imaging

Cells were covered with 60 μL of HEPES buffer and mounted on the microscope. A Carl Zeiss Axioplan II microscope (Carl Zeiss MicroImaging, Göttingen, Germany) equipped with a 63× magnification oil-immersion objective lens and a CCD camera C2400-75i (Hamamatsu Photonics, Hamamatsu City, Japan) was used for wide-field fluorescence imaging. The Zeiss Filterblock No. 01 (UV) was used. All measurements were carried out at room temperature.

RESULTS

Py-met-chol was obtained by the condensation of 1-pyrenecarboxaldehyde and pregnenolone according to Scheme 1 in the Supplementary Material, which also describes the organic synthesis and characteristics of all intermediary products, as well as the crystal data for tert-butyldimethylsilyl-(Py-met-chol) (Supplementary Material, Fig. S1). The structure and the emission and excitation fluorescence spectra of Py-met-chol are shown in Fig. 1. All emission spectra recorded during this study were similar to the spectrum shown in Fig. 1 *b*. The resolution and the wavelengths were unchanged: I_1 = 376 nm, I_3 = 388 nm and I_E = 475 nm, respectively.

To characterize the behavior of the pyrene probe in membranes, we studied vesicles composed of phosphatidylcholines (PC) with different acyl chains (DMPC, POPC, DOPC), mixed with a series of mole fractions of cholesterol.

Py-met-chol maximum solubility

We measured the maximum solubility of Py-met-chol in LUVs composed of POPC at room temperature and compared it to

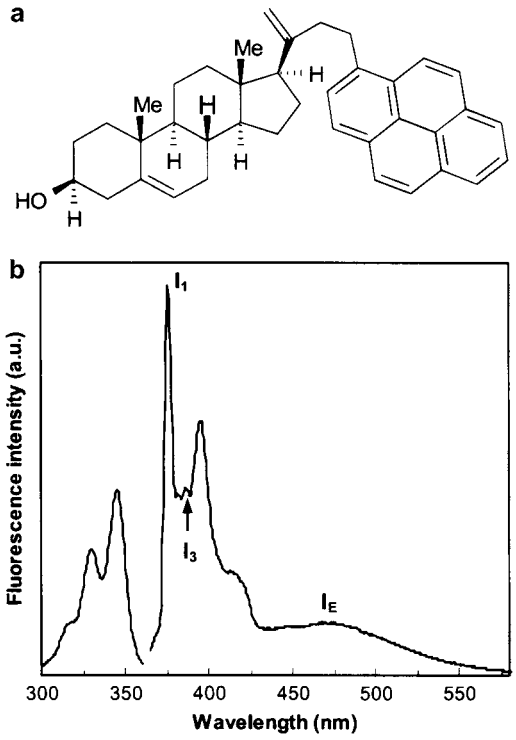

FIGURE 1 (*a*) Chemical structure of Py-met-chol (3β-hydroxy-pregn-5-ene-21-(1-methylpyrenyl)-20-methylidene). (*b*) Emission (*right*) (λ_{Em} = 330 nm, bandwidth 2 nm) and excitation (*left*) (λ_{Ex} = 388 nm, bandwidth 2 nm) fluorescence spectra in a bilayer: I_1, I_3, and I_E were measured at 376, 388, and 475 nm, respectively.

Py-ester-chol solubility and published results for cholesterol (22). The saturation of phospholipids with Py-met-chol was detected in absorption and fluorescence spectra: Py-met-chol aggregates in the buffer and leads to red-shifted absorption and excitation spectra (23,24) (data not shown). These aggregates were easily removed by centrifugation. Py-met-chol inserted into POPC LUVs was thus quantified by absorption measurements. We found that POPC LUVs are saturated with 28 ± 2 mol % of Py-met-chol at 20°C, a much higher value than for Py-ester-chol (~6 ± 1 mol %) (18).

Comparison of the effects of cholesterol and Py-met-chol on DPPC endotherms

We investigated by differential scanning calorimetry (DSC) the effect of cholesterol and Py-met-chol on the modification of the phase physical properties of saturated-PC MLVs. Representative DSC heating scans of aqueous multilamellar suspensions of DPPC containing 0, 2.1, 5, 10, 15, and 20 mol % of cholesterol or Py-met-chol are shown in Fig. 2, *a* and *b*. Pure DPPC exhibited a classical endotherm similar to that described in the literature (25): an endothermic pre-transition at 36°C followed by the main transition at 41.5°C. The main transition was abolished by 20 mol % of cholesterol and by 15 mol % of Py-met-chol. The variations of the main transition melting enthalpies as a function of sterol contents (0–20 mol %) revealed that the disturbance of the DPPC melting enthalpy was similar for the two sterols (Fig. 2 *c*).

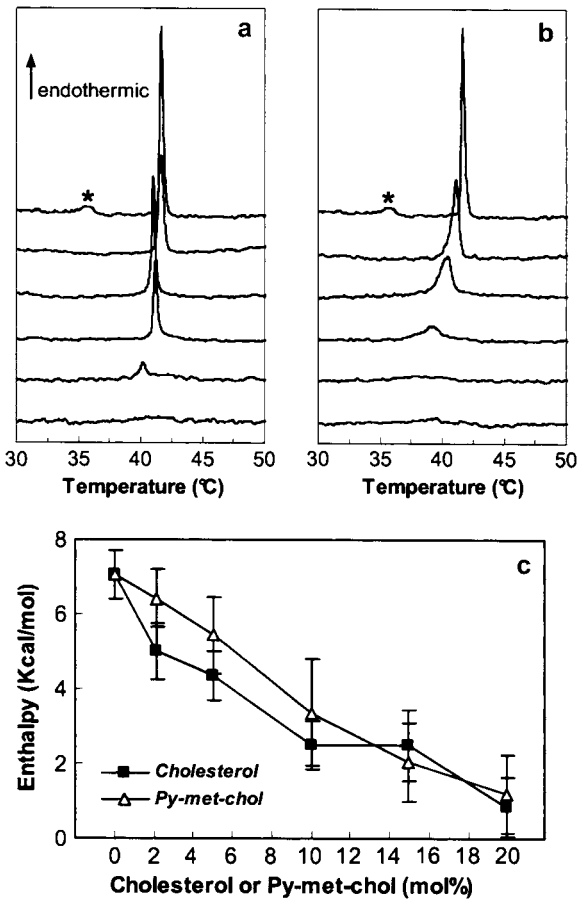

FIGURE 2 (*a* and *b*) Representative raw DSC scans at 30°C/h of DPPC MLVs with various cholesterol (*a*) or Py-met-chol (*b*) mole fractions. DPPC vesicles contained, from top to bottom, 0, 2.1, 5, 10, 15, and 20 mol %. The stars indicate the pretransition peak of the pure DPPC MLVs. (*c*) Effect of increasing amounts of cholesterol or Py-met-chol on the main-transition chain melting enthalpy.

Self-association of Py-met-chol in model membranes

We exploited the hypochromic behavior of pyrene to determine the lateral distribution of the ground-state Py-met-chol in fluid-phase LUVs according to the isodesmic self-associative model (see Appendix) (18). The molar absorption coefficients ε_{meas} were determined from the maximum absorption wavelength (corresponding to the lowest-energy band of the allowed $S_0 \rightarrow S_2$ pyrene transition: 345 nm) as a function of the probe to host lipid mole fraction (0.01–5 mol %). Measurements were made at 30°C in DMPC, POPC, and DOPC vesicles (characterized by different degrees of acyl-chain unsaturation) and LUVs constituted by two DMPC/cholesterol mixtures (85:15 and 70:30). Data and isodesmic fits are illustrated in Fig. 3. The ε_{meas} values for all liposome suspensions were ~32,000 M^{-1} cm^{-1} at 1 mol % of Py-met-chol and were little different at a probe mole fraction of 5 mol %. However, when we lowered the probe mole fraction the ε_{meas} values increased, indicating a hypochromic effect of the probe. This effect was observed more sharply in LUVs composed of unsaturated phospholipids. No shift of the maximum wavelength of pyrene absorption was detected.

To quantify this phenomenon, we used the generic Eq. A12 of the isodesmic model to fit the data and then determined the self-association constant, K (M^{-1}) and the molar absorption coefficients ε_{mono}, ε_{int}, and ε_{ext} (M^{-1} cm^{-1}) corresponding to the overall absorption process of these LUV suspensions (Table 1). In each case, the self-association process led to the formation of oligomers (*n*-mers) whose distribution and size were calculated according to Eqs. A7 and A8 for a given K value and various probes to host lipid mole fractions (C_T). This is illustrated in Fig. 4 using an association constant of 93 M^{-1}, corresponding to LUVs composed of pure DMPC: the calculated distributions for *n*-mers up to heptamers are shown. In Table 2 are reported, for the LUV suspensions studied, 1), the calculated size of the most abundant *n*-mer and the largest *n*-mer size (90% of probe molecules are expected to be in *n*-mers of this size or smaller), for 2, 5, 20, and 30 mol % of Py-met-chol; and 2), the percentages of the monomers for 2 mol % Py-met-chol. We noticed that the more the phospholipids are saturated, the more the probe was distributed as monomer. Similarly, the amount of monomer increased with the amount of cholesterol in DMPC.

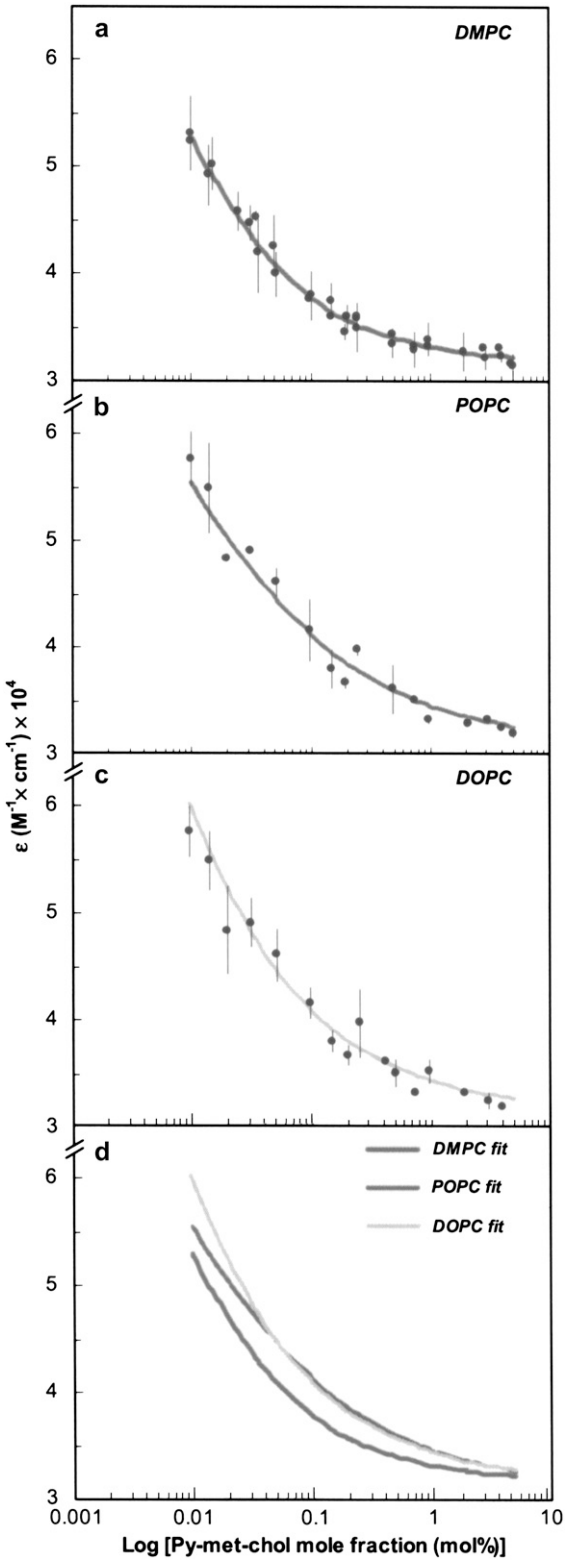

FIGURE 3 (*a–c*) Experimental data (*dots*) and corresponding isodesmic-based fits (*lines*) of Py-met-chol molar absorption coefficient as a function of probe mole fraction in LUVs of DMPC (*a*), POPC (*b*), and DOPC (*c*). (*d*) Superimposition of fitting curves. All measurements were performed above T_m (30°C). Error bars represent standard deviations of two independent experiments.

Fluorescence of Py-met-chol in model membranes

As cholesterol is able to induce a lo phase in some lipid membranes, thereby increasing the membrane thickness, we measured the fluorescence emission spectra of Py-met-chol in LUVs composed of DMPC, POPC, or DOPC with a series of amounts of cholesterol.

The percentage of probe labeling

Fig. 5 *a* shows I_3 and I_E intensities as a function of the probe mole fraction. A linear correlation between the probe quantity and I_3 was found in the concentration range of 0–1 mol % when there were few excimers. For LUVs containing >1 mol %, I_3 diverged from the linearity as I_E increased. We then tested 0.2, 0.5, or 2 mol % of Py-met-chol in DMPC with 0–55 mol % of cholesterol. The fluorescence intensities I_1, I_3, and I_E were measured and the ratios I_1/I_3 and I_E/I_3 calculated (Fig. 5, *b* and *c*). The sample with 2 mol % of Py-met-chol exhibited the maximum decrease of I_1/I_3 (30–35 mol % of cholesterol; Fig. 5 *b*), greater than that found for higher probe concentrations (data not shown). Above this mole fraction, I_1/I_3 increased with increasing cholesterol mole fractions and joined the other I_1/I_3 values (0.2–0.5 mol %). Similarly, I_E/I_3 only showed changes with the 2 mol % sample (Fig. 5 *c*): a constant and low value of I_E/I_3 was measured for mole fractions of cholesterol <30 mol %, but a steep continuous increase was observed between 30 and 55 mol %. The sudden variations of I_1/I_3 and I_E/I_3 at probe concentrations >30 mol % are due to the efficiency of the excimer's formation (see below). As excimer species are only detected at >1 mol % of probe, 2 mol % of Py-met-chol was used in the following experiments.

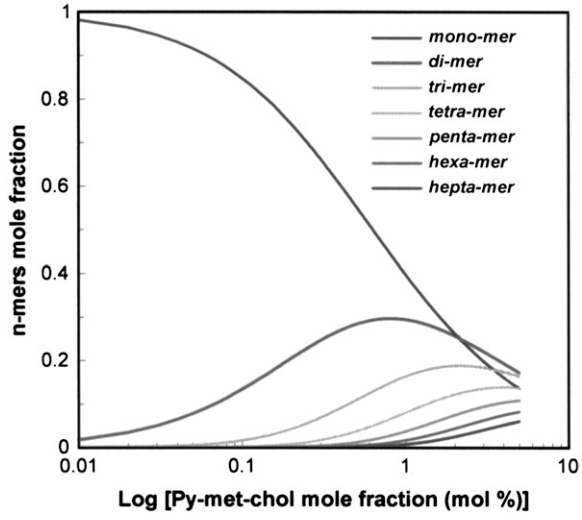

FIGURE 4 Calculated evolution of monomer to heptamer species as a function of Py-met-chol concentration in LUVs. We used an association constant value of 93 M^{-1}, which corresponds to a DMPC environment. Calculations were performed using the isodesmic model (see Appendix).

TABLE 1 Parameter values determined after data fitting according to the isodesmic model

		ε (M^{-1} cm^{-1})			
	K (M^{-1}) (95% CI)*	ε_{mono} (95% CI)*	ε_{ext} (95% CI)*	ε_{int} (95% CI)*	*n*
DOPC	669 (609–739)	143,510 (126,700–160,310)	70,750 (68,260–73,240)	31,360 (30,850–31,860)	33
POPC	281 (230–346)	77,270 (64,080–90,470)	61,860 (58,710–65,010)	31,020 (30,140–31,910)	31
DMPC	93 (84–103)	77,470 (74,260–80,690)	37,960 (36,750–39,170)	31,550 (31,030–32,070)	66
DMPC/chol (85:15)	68 (61–75)	74,450 (71,800–77,090)	34,940 (33,800–36,080)	31,220 (30,660–31,780)	36
DMPC/chol (70:30)	43 (38–49)	73,070 (71,350–73,780)	33,080 (32,300–33,870)	30,790 (29,360–31,200)	34

*Values in parentheses represent the 95% confidence intervals (CI), calculated as follows: for a given parameter (K, ε_{mono}, ε_{int}, or ε_{ext}), with all others fixed equal to the solution. Consequently, the 95% CI value corresponds to the range where the given parameter reduces the error by <5% (according to Fisher's test) on the $1/Y^2$-weighted residual sum of squares compared with the solution. ε values are rounded to the nearest tenth. *n*, number of samples.

Comparative study of DMPC, POPC, and DOPC LUVs with various concentrations of cholesterol and 2 mol % of Py-met-chol

In model membranes, cholesterol induces various lipid organizations (lo versus ld phases), so we verified that the probe was sensitive to these distinct membrane organizations. The normalized fluorescence ratios I_1/I_3 and I_E/I_3 are plotted against the mole fraction of cholesterol in Fig. 6, *a* and *b*. Only DMPC showed a significant decrease of I_1/I_3 until the mole fraction of cholesterol reached 30–35 mol %; this was followed by a partial recovery for higher concentrations of cholesterol. In DOPC and POPC there was less of a decrease. I_E/I_3 was unchanged in a range of 0–25 mol % of cholesterol (Fig. 6 *b*), but showed a considerable increase from 30 mol % in DMPC, a small increase from 45 mol % in POPC, and no variation in DOPC. The main difference between these LUVs containing 2 mol % of probe was that at 30 mol % of cholesterol and beyond, only DMPC is in lo phase, whereas >45 mol % of cholesterol is needed for POPC to display a lo phase. The lo lipid phase, its polarity decrease (due to its being less permeable to water than the ld phase), and the thickness increase were correlated (see below).

Fluorescence of Py-met-chol in plasma membranes

Py-met-chol was introduced into the plasma membrane of living CHO cells using a MβCD-based protocol. This protocol is easy to use, fast, and minimally disruptive. Trypan blue was used to measure cell viability from 2 to 24 h after cell labeling. Control and labeled cells multiplied and survived similarly (data not shown), indicating that Py-met-chol displayed no significant toxicity for living cells. Fig. 7 *a* shows a wide-field microscope image of Py-met-chol-labeled CHO-δ cells. The corresponding cell suspension fluorescence spectrum is illustrated in Fig. 7 *b* and shows a resolution comparable to that of LUV spectra. As deduced from model membranes, a qualitative analysis of the amount of inserted probe in the membrane is possible by considering I_E and I_E/I_3 values. Hence, the incubation time was adapted to give cell fluorescence spectra similar to those of liposomes composed of POPC/30 mol % cholesterol and containing 2 mol % of Py-met-chol. Indeed, the initial I_E/I_3 value measured was 0.33 $\pm$ 0.05 for all cell suspensions (Fig. 8 *a*) close to the 0.30 $\pm$ 0.01 obtained with POPC/30 mol % of cholesterol LUVs (see Fig. 6 legend for other data values).

We monitored the plasma membrane thickness change induced by agonist activation of mDOR (10). Fig. 8, *a* and *b*, shows the variations of I_E/I_3 and I_1/I_3 for CHO-wt and CHO-δ cells as a function of time after addition of buffer, Deltorphin II (mDOR agonist), or Diprenorphin (mDOR antagonist). With CHO-δ, a transient decrease of I_1/I_3 was observed 2 min after agonist addition, reaching a maximum magnitude after 4 min. Then, 2 min later, it had returned to its initial value and remained constant. I_1/I_3 did not change either in CHO-δ cells after addition of antagonist or buffer in CHO-wt (without mDOR) after agonist addition, showing the specific Deltorphin II-induced effect. This result is

TABLE 2 Calculated *n*-mer distributions for various probe mole fractions and association constants in liposomes

		Probe mole percentage (mol %)				
	K (M^{-1})	2	2	5	20	30
		Monomer (%)	(Majority *n*-mer*/largest *n*-mer†)			
DOPC	669	5.7	(4/14)	(6/22)	(12/45)	(14/55)
POPC	281	12	(2/9)	(4/14)	(8/29)	(9 36)
DMPC	93	26	(1/5)	(2/8)	(4/16)	(5/21)
DMPC/chol (85:15)	68	68	(1/4)	(2/7)	(4/14)	(5/17)
DMPC/chol (70:30)	43	93	(1/3)	(2/5)	(3/11)	(4/14)

*The majority *n*-mer is the one with the highest mole fraction in the liposome.
†The largest *n*-mer size, describing 90% of probe molecules.

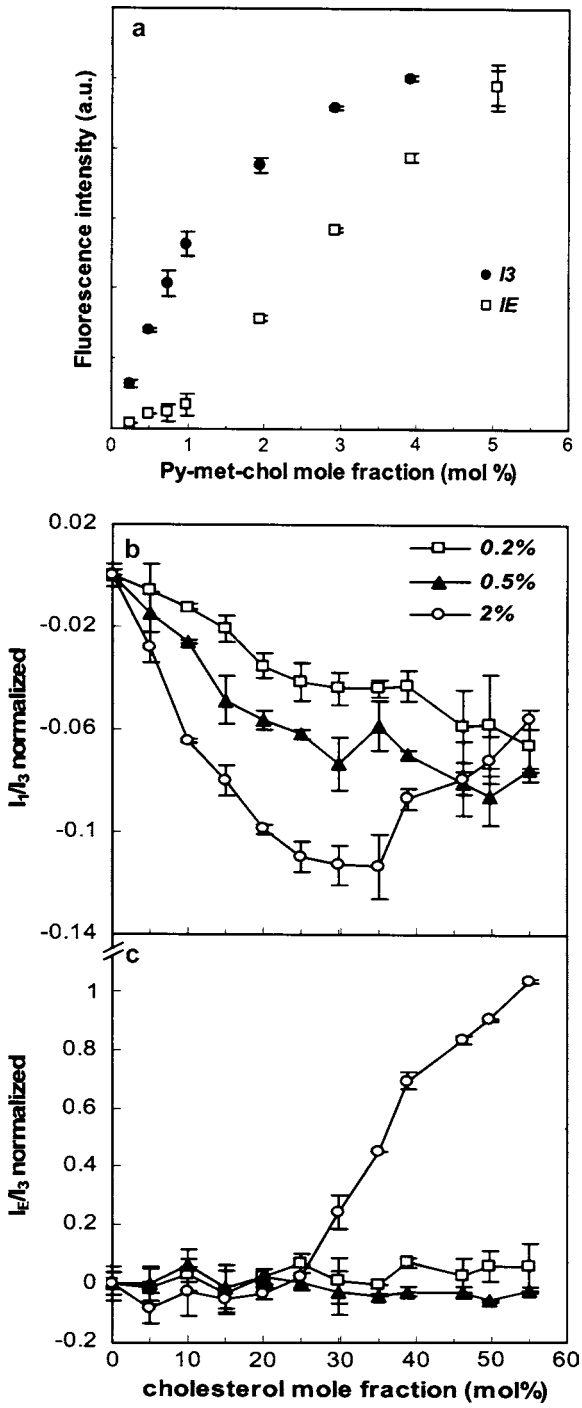

FIGURE 5 (*a*) Fluorescence intensities of the monomer (I_3, 388 nm) and the excimer (I_E, 475 nm) as a function of Py-met-chol mole fraction, in LUVs of DMPC. Fluorescence ratios I_1/I_3 (*b*) and I_E/I_3 (*c*) of Py-met-chol incorporated at 0.2, 0.5, or 2 mol % in LUVs composed of DMPC as a function of cholesterol mole fraction. Ratios are normalized taking ratio values for suspensions without cholesterol as the reference, which corresponded to I_1/I_3 and I_E/I_3 values of: 1.82 and 0.06 with 0.2 mol % of Py-met-chol, 1.89 and 0.15 with 0.5 mol %, and 1.99 and 0.27 with 2 mol %. Error bars represent standard deviations of two independent experiments. In all cases, the temperature was 37°C.

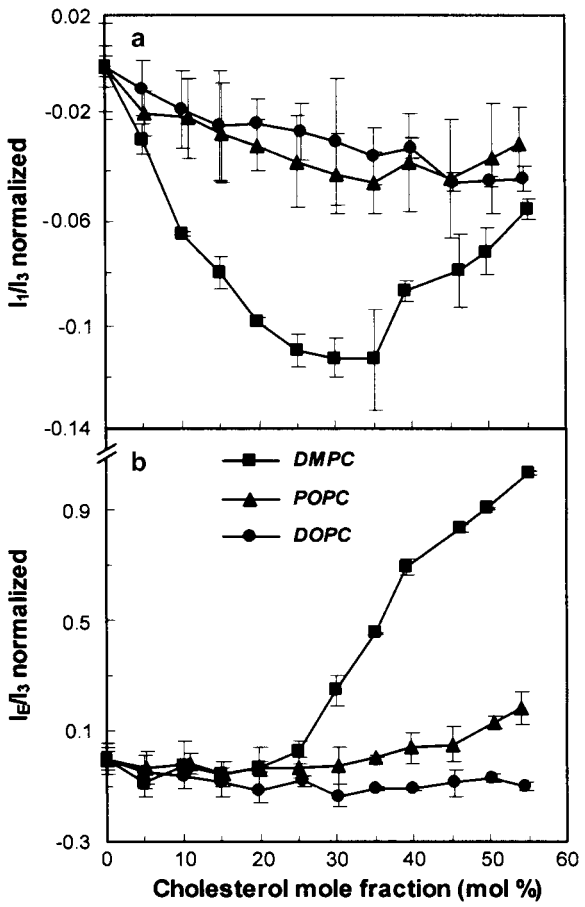

FIGURE 6 Fluorescence of Py-met-chol incorporated at 2 mol % in LUVs of DMPC, POPC, and DOPC as a function of cholesterol mole fraction. Evolution of I_1/I_3 (*a*) and I_E/I_3 (*b*) ratios of Py-met-chol are shown. All measurements were performed at 37°C. Ratios are normalized taking ratio values for suspensions without cholesterol as the reference, which corresponded to the following values for I_1/I_3 and I_E/I_3: 1.98 ± 0.01 and 0.27 ± 0.01 in DMPC, 1.99 ± 0.01 and 0.30 ± 0.01 in POPC, and 2.02 ± 0.01 and 0.35 ± 0.01 in DOPC.

strengthened by the observation of an absence of change of I_1/I_3 and I_E/I_3 after addition of 1 μM of these ligands in LUV suspensions of DMPC containing 0 or 30 mol % of cholesterol and labeled with 2 mol % of Py-met-chol.

DISCUSSION

We report that Py-met-chol, owing to its structure, is much more soluble than Py-ester-chol in model membranes. Although this solubility is lower than that of cholesterol in POPC (66 mol % (22)), our probe is able to label natural membranes using MβCD. The low MβCD concentration used (2.5 mM) is not sufficient to induce cholesterol depletion from the plasma membrane (26). Moreover, the labeling conditions (only 2 min at 37°C) are safe for living cells. First, we compared the behavior of Py-met-chol and cholesterol.

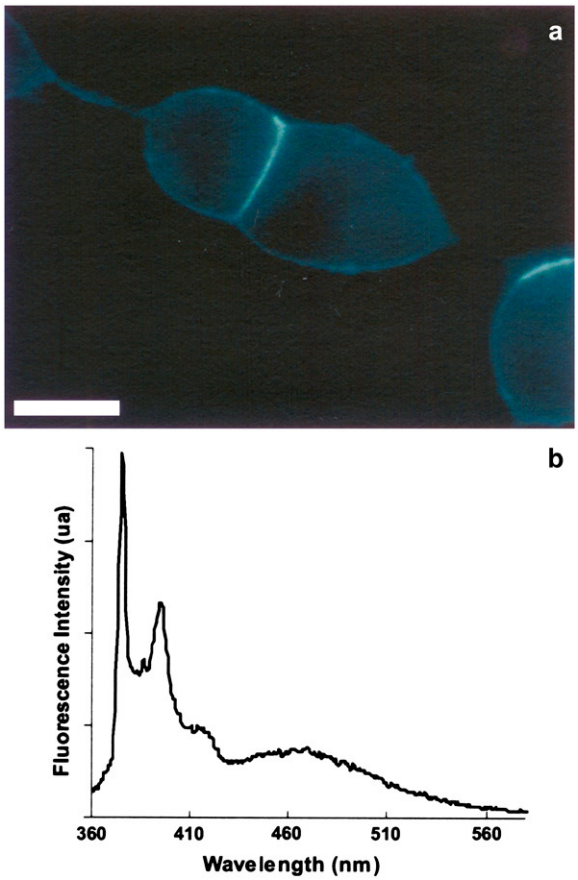

FIGURE 7 Fluorescence of Py-met-chol in living cells. (*a*) Wide-field microscope fluorescence image of plasma membranes of CHO-δ cells incubated with Py-met-chol/MβCD for 2 min at 37°C. The samples were observed at room temperature. Scale bar, 10 μm. (*b*) Emission spectrum of a CHO-δ cell suspension at 37°C labeled with Py-met-chol.

Biophysical behavior and absorbance properties of Py-met-chol in model membranes

The effects of cholesterol and Py-met-chol on saturated phosphatidylcholine MLV endotherms were determined. DPPC was selected for the abundance and diversity of the data in the literature. T_m (Fig. 2, *a* and *b*) changed slightly when Py-met-chol replaced cholesterol ($\Delta T \approx -4$°C and -1°C, respectively, at 10 mol %). These decreases indicated better sterol solubility in the fluid phase than in the gel phase. The broadening of the main transition peak revealed a lesser DPPC melting cooperativity for Py-met-chol than for cholesterol. The melting enthalpies of this transition decreased in a comparable way to, and linearly with, the mole fractions of both cholesterol and Py-met-chol. These results suggest that Py-met-chol/DPPC interactions are likely to be determined by the cholesterol moiety of the probe. The DPPC endotherms with 2.1 mol % of Py-met-chol were comparable to those of DPHpPC, a probe known for its limited disruptive effect on saturated PC (27). These various findings indicate that the pyrene moiety has a little effect on lipid membranes, especially if its concentration does not exceed 2 mol %.

We determined the lateral distribution of Py-met-chol at 30°C in the ground state by measuring the molar absorption coefficients, ε_{meas}, at the maximum absorption wavelength of the $S_0 \rightarrow S_2$ pyrene transition, as a function of the probe concentration (18). A hypochromic effect was observed in all LUV suspensions as the Py-met-chol concentration increased. According to Todesco et al. (28), this suggests that stacking of pyrene chromophore occurs and is a function of the probe concentration. We used an isodesmic model to estimate the self-association constants, K, and the theoretical molar absorption coefficients ε_{mono}, ε_{int}, and ε_{ext}. We found that $\varepsilon_{mono} > \varepsilon_{ext} > \varepsilon_{int}$, and for the five distinct classes of LUVs studied, ε_{int} values are in the same range. This leads to converging ε_{meas} values (close to ε_{int}) in LUVs when the probe concentration is >1 mol % (Fig. 3). The contribution of ε_{mono} is higher when the probe concentration is lower, but ε_{meas} never reached values close to ε_{mono} because this would correspond to LUVs containing too few probe molecules to be detected (i.e., probe concentration <0.01 mol %). Moreover, we report that $K_{DOPC} > K_{POPC} > K_{DMPC}$, corresponding to increased probe self-association as the degree of acyl-chain unsaturation increases. This effect is comparable to the cholesterol interaction with phosphatidylcholines, which is favored when acyl chains are saturated (29). The calculations of n-mer distributions for various percentages of Py-met-chol reveal the efficiency of this self-associative process as assessed from the stack sizes: at 2 mol % of probe, monomers were prevalent in DMPC, whereas tetramers were the majority form in DOPC. Our findings with DMPC liposomes containing 2 mol % of Py-met-chol and mixed with 0, 15, or 30 mol % of cholesterol (Table 1) show that K decreases as the cholesterol mole fraction increases. This can be explained by better probe solvation in DMPC/cholesterol than in pure DMPC LUVs. Indeed, we found that for 2 mol % of probe, 93% of Py-met-chol molecules were monomeric in DMPC/cholesterol (70:30) LUVs, but only 26% were monomers in pure DMPC.

Previous studies analyzing cholesterol solubility in various types of lipids have arrived at the same conclusion. Effectively, the phase behavior of binary mixtures containing cholesterol and phospholipids indicated nonideal mixing of cholesterol and the presence of ld/lo immiscibility regions (30–32), and cholesterol promotes the lo domain (33). Furthermore, the acyl-chain structure is known to affect cholesterol interaction with lipids (34), causing variations in cholesterol distribution and membrane dynamics. Radhakrishnan et al. (35) reported that there is less evidence for cholesterol complex formation with unsaturated than with saturated PC. This suggests that cholesterol is better solvated in saturated than in unsaturated lipid environments where it is partially excluded, implying formation of cholesterol oligomers rather than monomers (34).

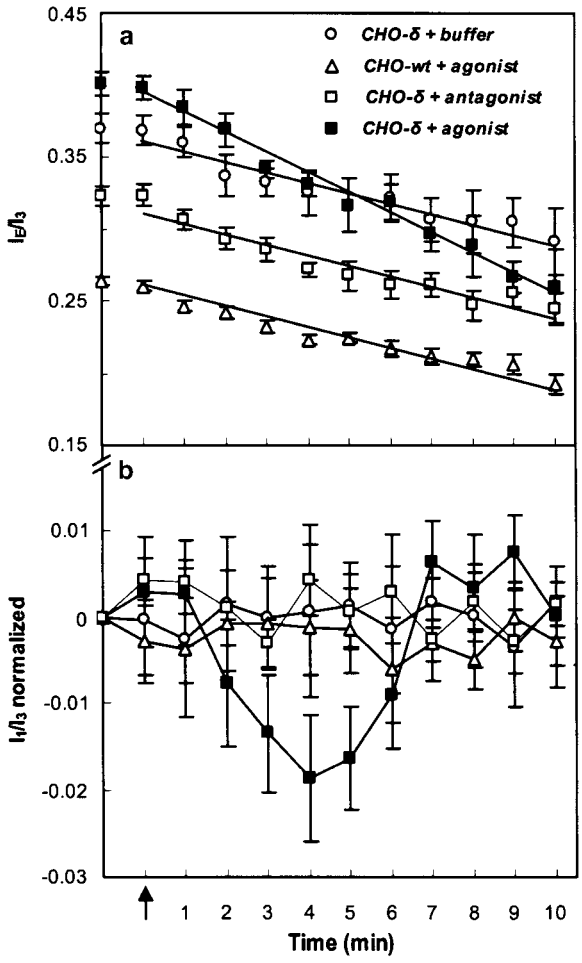

FIGURE 8 Fluorescence I_E/I_3 values of one set of various conditions (*a*) and normalized I_1/I_3 values for all experiments (*b*) involving Py-met-chol with living CHO-δ and CHO-wt cell suspensions. The arrow indicates the addition to the CHO-δ cell suspension of a solution of buffer (HEPES, $n = 9$), antagonist (Diprenorphin, $n = 10$), or agonist (Deltorphin II, $n = 11$), or addition of a solution of agonist to the CHO-wt cell suspension ($n = 10$). I_1/I_3 ratios are normalized taking ratio values measured before ligand addition. Error bars correspond to mean ± SE of n experiments. Agonist and antagonist were used at final concentrations of 1 μM. All measurements were carried out at 37°C. Lines are provided to facilitate reading.

Our results with Py-met-chol after absorption measurements and isodesmic fitting confirm these findings for cholesterol, with, in addition, a quantification of the lateral distribution of the probe. It may be possible to extrapolate this lateral distribution to that of cholesterol. Similar patterns for the lateral distribution of cholesterol were proposed after dynamic simulations of particular lipid/cholesterol mixtures (36). Mazères et al. (37) used a similar experimental approach based on pyrene-labeled phospholipids and reported weaker K values (<1 M^{-1}) than those determined with Py-ester-chol (18) or Py-met-chol (Table 1). These various results suggest that the cholesterol moiety induces the stacking of cholesterol-pyrene probe.

Fluorescence properties of Py-met-chol in model membranes

Fluorescence measurements justified the choice of 2 mol % for optimum labeling, because 1), this is near the limit of the linear relationship between the fluorescence monomer intensity and the Py-met-chol concentration (Fig. 5); 2), it generates the largest amplitude of I_1/I_3 variations (Figs. 5 *b* and 6 *a*); and 3), it allows an accurate quantification of the excimer (Fig. 5). Furthermore, absorbance findings show that the most abundant n-mer is the monomer in DMPC samples at 2 mol % of probe (Fig. 4 and Table 2), allowing an assessment of membrane polarity (15,38).

We carried out fluorescence studies of Py-met-chol incorporated into DMPC, POPC, and DOPC LUVs with a series of concentrations of cholesterol (Fig. 6, *a* and *b*). A correlation between the probe fluorescence and the physical properties of the membrane was observed. Note that at >30 mol % of cholesterol in DMPC, a full lo phase is present (39); hence, the thickness of the membrane is maximum (9), and the molecular protrusion of lipids is reduced (0.7 Å with 30 mol % of cholesterol and 2.7 Å in pure DMPC) (40). This leads to a much lower polarity of the lipid core than the ld phase, because the restricted conformational and rotational motions do not allow the water to cross the membrane with the same efficiency as in an ld lipid phase (41). This explains our results with DMPC, where biphasic behavior is observed: a decrease of I_1/I_3 until a full lo phase occurs, followed by a recovery toward the POPC and DOPC I_1/I_3 values. These I_1/I_3 changes were not found with POPC or DOPC. For DOPC, cholesterol is known not to promote a lo phase but can induce only higher-order acyl chains (42). In contrast, for POPC, a single lo phase should be present above ~45 mol % of cholesterol (43). Perhaps the small increase of I_1/I_3 above 45 mol % of cholesterol (Fig. 6 *a*) reflects this phenomenon. The same biphasic behavior is clearly observed for I_E/I_3 with DMPC, whereas I_E/I_3 remains constant in DOPC and increases very slightly in POPC (Fig. 6 *b*). In all LUVs, from 0 to 25 mol % of cholesterol, I_E/I_3 values are comparable but when the full lo phase is reached, an increase is observed. This is a consequence of an increasing number of monomers, as revealed by absorbance data (93% of monomers versus 26% without cholesterol (see Table 2)), inducing a more effective excimer formation (44). Indeed, as reported in many studies, excimer formation is a dynamic process and excimers are not formed from ground-state oligomers in a bilayer (45). The increase of I_E/I_3 in the DMPC lo phase as the cholesterol concentration increases supports this statement. However, this effect is probably slowed because the diffusion coefficient of the lo phase is smaller than that of the ld phase (46).

These various findings confirm that 1), the probe has better miscibility in the lo phase than in the ld phase; 2), the I_E/I_3 ratio can be used as an indicator to distinguish ld from full lo phase in model membranes; and 3), I_1/I_3 is a sensitive

indicator of membrane polarity when fluid ld and lo phases coexist.

Fluorescence properties of Py-met-chol in the plasma membrane of living cells

The fluorescence spectra of Py-met-chol in living cell membranes (Fig. 7 *b*) showed a resolution comparable to those of LUVs (Fig. 1 *b*). An initial I_E/I_3 value of 0.33 ± 0.05 confirmed that the Py-met-chol quantity inserted into cell plasma membranes was in accordance with our labeling criterion. Nevertheless, initial I_1/I_3 values were in the range of 2.15–2.30, and thus different from initial I_1/I_3 values of LUVs containing 30 mol % of cholesterol (1.75–1.95). This indicates that the probe environment inside the plasma membrane is more polar than that inside model membranes. This could be the result of polar atoms brought by transmembrane proteins into cell membranes.

Unlike LUVs, decreases of I_E/I_3 in living cells were observed during the observation time. Indeed, in living cells, endocytosis and exocytosis exchanges occur, leading to a permanent efflux from the plasma membrane. However, this decrease was greater in the CHO-δ incubated with the agonist (Fig. 8 *a*) than in controls, because a supplementary process takes place: the internalization of the mDOR to regulate its function (47).

The kinetics of I_1/I_3 variations revealed different behaviors according to cell stimulation (Fig. 8 *b*). Various findings and concepts have to be considered to interpret these results. Some GPCRs modify the thickness of the surrounding membrane as part of their signaling function: rhodopsin and DOR specifically change their transmembrane conformation after agonist binding, as revealed by surface plasmon resonance studies (10,48), inducing an increase in the transmembrane thickness. These changes may induce a hydrophobic mismatch between the protein and the surrounding lipids (49,50), which could be a driving force for variations of local concentrations of particular lipids (including cholesterol), and for thickness adaptations of lipid acyl chains (51). This thickness increase inevitably reduces the water permeability and the correlated intrinsic membrane polarity. By measuring Py-met-chol I_1/I_3 fluorescence, we observed a transient and specific change with mDOR after agonist binding. The timing of this biphasic I_1/I_3 change (a signal diminution for 4 min followed by a recovery to the initial value after 10 min), is consistent with the characteristic times of two opposite processes, the internalization (47) and recycling (52) mechanisms of mDOR. Note that with respect to the I_1/I_3 and I_E/I_3 variations in LUVs, which account for the entire membrane, the variation in cells corresponded to membrane subfractions occupied by the mDOR transmembrane protein.

We point out that our results were observed in living cells. Furthermore, mDOR has been inserted in LUVs of defined compositions, but we were never able to reconstitute it in a high-affinity state to observe the binding of agonists, even though this GPCR was characterized as inserted into the lipid phase of these LUVs (data not shown). This underlines the great difficulties encountered in reconstructing active GPCRs in model membranes.

However, our observations confirmed that Py-met-chol fluorescence measurements in living cells can be used as a sensitive indicator to follow induced lipid organization changes.

In conclusion, we have synthesized a new fluorescent probe derived from cholesterol and have demonstrated that, in membranes, it can 1), report on the lateral distribution of cholesterol; 2), from I_1/I_3, measure polarity changes in the hydrophobic core of model membranes; 3), from I_E/I_3, characterize the lo phase in model membranes; and 4), reveal lipid organization changes specifically induced by agonist binding to mDOR. This new cholesterol-pyrene probe could be used for screening analyses of new GPCR ligands in living cells (53), when the transmembrane protein conformational changes induced by their activation are comparable to that of mDOR.

APPENDIX

Self-associative model (18): Assuming an infinite linear self-association scheme in which each step is characterized by the same equilibrium constant K, only three kinds of contribution are expected to account for the absorption properties of pyrene probes: the molar extinction coefficients of free monomers (ε_{mono}), and, in a stack of n-mers, the contributions of both (n-2) internal (ε_{int}) and the two external (ε_{ext}) units. The calculated molar absorption coefficient ε_{calc} for a given probe concentration is:

$$\varepsilon_{calc} = \alpha_{mono} \times \varepsilon_{mono} + \alpha_{ext} \times \varepsilon_{ext} + \alpha_{int} \times \varepsilon_{int}, \tag{A1}$$

$$\text{with} \quad \alpha_{mono} + \alpha_{ext} + \alpha_{int} = 1 \tag{A2}$$

where α_{mono}, α_{ext}, and α_{int} are the molar fractions of free monomers and those of probes at the extremities and inside the stacks, respectively, and correspond to

$$\alpha_{mono} = \frac{[Py_1]}{C_T}; \tag{A3}$$

$$\alpha_{ext} = \sum_{i=2}^{\infty} \frac{2 \times [Py_i]}{C_T}; \tag{A4}$$

and

$$\alpha_{int} = \sum_{i=2}^{\infty} \frac{(i-2) \times [Py_i]}{C_T}, \tag{A5}$$

where $[Py_i]$ is the molar fraction of n-mers consisting of i pyrene-probe molecules, $[Py_1]$ is the molar fraction of monomer, and C_T the probe/host lipid mole fraction. Applying mass conservation, we have

$$C_T = \sum_{i=1}^{\infty} [Py_i] \times i. \tag{A6}$$

Accordingly, the equation used to calculate individual molar concentrations of n-mers is

$$[Py_i] = i \times K^{i-1} \times [Py_1]^i, \tag{A7}$$

and so the relationship between C_T, $[Py_1]$, and K can be interpreted as

$$[\mathrm{Py}_1] = \frac{1}{K} + \frac{1 - \sqrt{4C_\mathrm{T} \times K + 1}}{2K^2 \times C_\mathrm{T}}, \quad \text{(A8)}$$

and we can then write

$$\alpha_\mathrm{mono} = \frac{1}{K \times C_\mathrm{T}} + \frac{1 - \sqrt{4C_\mathrm{T} \times K + 1}}{2K^2 \times C_\mathrm{T}^2}; \quad \text{(A9)}$$

$$\alpha_\mathrm{int} = -\frac{C_\mathrm{T} - [\mathrm{Py}_1]}{C_\mathrm{T}} + 2 \times \frac{K \times [\mathrm{Py}_1]^2}{C_\mathrm{T} \times (1 - K \times [\mathrm{Py}_1])^2}; \quad \text{(A10)}$$

and

$$\alpha_\mathrm{ext} = 2 \times \frac{C_\mathrm{T} - [\mathrm{Py}_1]}{C_\mathrm{T}} - \frac{2K \times [\mathrm{Py}_1]^2}{C_\mathrm{T} \times (1 - K \times [\mathrm{Py}_1])^2}. \quad \text{(A11)}$$

The generic equation of the isodesmic model is obtained by introducing the Eqs. A8–A11 into Eq. A1, giving

$$\varepsilon_\mathrm{calc} = {}^{f}K, \varepsilon_\mathrm{mono}, \varepsilon_\mathrm{int}, \varepsilon_\mathrm{ext}^{(C_\mathrm{T})}. \quad \text{(A12)}$$

Knowing C_T and using the above equations, we were able to calculate, by an iterative process, α_mono, α_ext, and α_int and determine the best values for the various parameters—K, $\varepsilon_\mathrm{mono}$, ε_ext, and ε_int—shown in Table 1. Equations A7 and A8 led to descriptions of n-mer distributions as a function of the host lipid/probe molar fractions shown in Fig. 4.

SUPPLEMENTARY MATERIAL

To view all of the supplemental files associated with this article, visit www.biophysj.org.

This work was supported by the Centre National de la Recherche Scientifique and the Association pour la Recherche contre le Cancer. L.G. was supported by a grant from Fonds Social Européen.

REFERENCES

1. Pike, L. J. 2003. Lipid rafts: bringing order to chaos. *J. Lipid Res.* 44: 655–667.
2. Brown, D. A., and E. London. 1998. Structure and origin of ordered lipid domains in biological membranes. *J. Membr. Biol.* 164:103–114.
3. Simons, K., and D. Toomre. 2000. Lipid rafts and signal transduction. *Nat. Rev. Mol. Cell Biol.* 1:31–39.
4. London, E., and D. A. Brown. 2000. Insolubility of lipids in triton X-100: physical origin and relationship to sphingolipid/cholesterol membrane domains (rafts). *Biochim. Biophys. Acta.* 1508:182–195.
5. Schuck, S., M. Honsho, K. Ekroos, A. Shevchenko, and K. Simons. 2003. Resistance of cell membranes to different detergents. *Proc. Natl. Acad. Sci. USA.* 100:5795–5800.
6. Brown, D. A., and E. London. 2000. Structure and function of sphingolipid- and cholesterol-rich membrane rafts. *J. Biol. Chem.* 275: 17221–17224.
7. Brown, D. A., and E. London. 1998. Functions of lipid rafts in biological membranes. *Annu. Rev. Cell Dev. Biol.* 14:111–136.
8. Ikonen, E. 2001. Roles of lipid rafts in membrane transport. *Curr. Opin. Cell Biol.* 13:470–477.
9. Gandhavadi, M., D. Allende, A. Vidal, S. A. Simon, and T. J. McIntosh. 2002. Structure, composition, and peptide binding properties of detergent soluble bilayers and detergent resistant rafts. *Biophys. J.* 82:1469–1482.
10. Salamon, Z., V. J. Hruby, G. Tollin, and S. Cowell. 2002. Binding of agonists, antagonists and inverse agonists to the human δ-opioid receptor produces distinctly different conformational states distinguishable by plasmon-waveguide resonance spectroscopy. *J. Pept. Res.* 60: 322–328.
11. Barrow, D. A., and B. R. Lentz. 1985. Membrane structural domains. Resolution limits using diphenylhexatriene fluorescence decay. *Biophys. J.* 48:221–234.
12. Nyholm, T., M. Nylund, A. Soderholm, and J. P. Slotte. 2003. Properties of palmitoyl phosphatidylcholine, sphingomyelin, and dihydrosphingomyelin bilayer membranes as reported by different fluorescent reporter molecules. *Biophys. J.* 84:987–997.
13. Duportail, G., and P. Lianos. 1996. Fluorescence probing of lipid vesicles using pyrene and pyrene derivatives. M. Rosoff, editor. Surfactant Science series, New York.
14. Barenholz, Y., T. Cohen, E. Haas, and M. Ottolenghi. 1996. Lateral organization of pyrene-labeled lipids in bilayers as determined from the deviation from equilibrium between pyrene monomers and excimers. *J. Biol. Chem.* 271:3085–3090.
15. L'Heureux, G. P., and M. Fragata. 1987. Micropolarities of lipid bilayers and micelles. 4. Dielectric constant determinations of unilamellar phosphatidylcholine vesicles. *J. Colloid Interface Sci.* 117:513–522.
16. Subczynski, W. K., A. Wisniewska, J. J. Yin, J. S. Hyde, and A. Kusumi. 1994. Hydrophobic barriers of lipid bilayer membranes formed by reduction of water penetration by alkyl chain unsaturation and cholesterol. *Biochemistry.* 33:7670–7681.
17. Pérochon, E., A. Lopez, and J. F. Tocanne. 1992. Polarity of lipid bilayers. A fluorescence investigation. *Biochemistry.* 31:7672–7682.
18. Lagane, B., S. Mazères, C. Le Grimellec, L. Cézanne, and A. Lopez. 2002. Lateral distribution of cholesterol in membranes probed by means of a pyrene-labelled cholesterol: effects of acyl chain unsaturation. *Biophys. Chem.* 95:7–22.
19. Dittmer, J. C., and R. L. Lester. 1964. A simple, specific spray for the detection of phospholipids on thin-layer chromatograms. *J. Lipid Res.* 15:126–127.
20. Zak, B., R. C. Dickenman, E. G. White, H. Burnett, and P. J. Cherney. 1954. Rapid estimation of free and total cholesterol. *Am. J. Clin. Pathol.* 24:1307–1315.
21. Bullova, H., and P. Balgavy. 2005. Turbidimetric study of unilamellar extruded egg phosphatidylcholine liposomes. *Acta Fac. Pharm. Univ. Comen.* 52:66–71.
22. Huang, J., J. T. Buboltz, and G. W. Feigenson. 1999. Maximum solubility of cholesterol in phosphatidylcholine and phosphatidylethanolamine bilayers. *Biochim. Biophys. Acta.* 1417:89–100.
23. Prodi, L., R. Ballardini, M. T. Gandolfi, and R. Roversi. 2000. A simple fluorescent chemosensor for alkaline-earth metal ions. *J. Photochem. Photobiol. Chem.* 136:49–52.
24. Yang, J. S., C. S. Lin, and C. Y. Hwang. 2001. Cu^{2+}-induced blue shift of the pyrene excimer emission: a new signal transduction mode of pyrene probes. *Org. Lett.* 3:889–892.
25. McMullen, T. P., and R. N. McElhaney. 1995. New aspects of the interaction of cholesterol with dipalmitoylphosphatidylcholine bilayers as revealed by high-sensitivity differential scanning calorimetry. *Biochim. Biophys. Acta.* 1234:90–98.
26. Christian, A. E., M. P. Haynes, M. C. Phillips, and G. H. Rothblat. 1997. Use of cyclodextrins for manipulating cellular cholesterol content. *J. Lipid Res.* 38:2264–2272.
27. Parente, R. A., and B. R. Lentz. 1985. Advantages and limitations of 1-palmitoyl-2-[[2-[4- (6-phenyl-trans-1,3,5-hexatrienyl)phenyl]ethyl]-carbonyl]-3-*sn*-phosphatidylcholine as a fluorescent membrane probe. *Biochemistry.* 24:6178–6185.
28. Todesco, R. V., R. A. Basheer, and P. V. Kamat. 1986. Photophysical and photochemical behavior of poly(1-vinylpyrene). Evidence for dual excimer fluorescence. *Macromolecules.* 19:2390–2397.
29. Ohvo-Rekila, H., B. Ramstedt, P. Leppimaki, and J. P. Slotte. 2002. Cholesterol interactions with phospholipids in membranes. *Prog. Lipid Res.* 41:66–97.

30. Sankaram, M. B., and T. E. Thompson. 1990. Modulation of phospholipid acyl chain order by cholesterol. A solid-state 2H nuclear magnetic resonance study. *Biochemistry*. 29:10676–10684.

31. Vist, M. R., and J. H. Davis. 1990. Phase equilibria of cholesterol/dipalmitoylphosphatidylcholine mixtures: 2H nuclear magnetic resonance and differential scanning calorimetry. *Biochemistry*. 29:451–464.

32. McMullen, T. P. W., and R. N. McElhaney. 1996. Physical studies of cholesterol-phospholipid interactions. *Curr. Opin. Colloid Interface Sci.* 1:83–90.

33. Silvius, J. R., D. del Giudice, and M. Lafleur. 1996. Cholesterol at different bilayer concentrations can promote or antagonize lateral segregation of phospholipids of differing acyl chain length. *Biochemistry*. 35:15198–15208.

34. Kusumi, A., W. K. Subczynski, M. Pasenkiewicz-Gierula, J. S. Hyde, and H. Merkle. 1986. Spin-label studies on phosphatidylcholine-cholesterol membranes: effects of alkyl chain length and unsaturation in the fluid phase. *Biochim. Biophys. Acta*. 854:307–317.

35. Radhakrishnan, A., and H. M. McConnell. 2000. Chemical activity of cholesterol in membranes. *Biochemistry*. 39:8119–8124.

36. Subczynski, W. K., and A. Kusumi. 2003. Dynamics of raft molecules in the cell and artificial membranes: approaches by pulse EPR spin labeling and single molecule optical microscopy. *Biochim. Biophys. Acta*. 1610:231–243.

37. Mazères, S., B. Lagane, M. Welby, V. Trégou, and A. Lopez. 2001. Probing the lateral organization of membranes: fluorescence repercussions of pyrene probe distribution. *Spectrochim. Acta A Mol. Biomol. Spectrosc*. 57:2297–2311.

38. L'Heureux, G. P., and M. Fragata. 1988. Micropolarities of lipid bilayers and micelles. 5. Localization of pyrene in small unilamellar phosphatidylcholine vesicles. *Biophys. Chem.* 30:293–301.

39. Almeida, P. F., W. L. Vaz, and T. E. Thompson. 1992. Lateral diffusion in the liquid phases of dimyristoylphosphatidylcholine/cholesterol lipid bilayers: a free volume analysis. *Biochemistry*. 31: 6739–6747.

40. Douliez, J. P., A. Leonard, and E. J. Dufourc. 1996. Conformational order of DMPC *sn*-1 versus *sn*-2 chains and membrane thickness: an approach to molecular protrusion by solid-state 2H-NMR and neutron diffraction. *J. Phys. Chem*. 100:18450–18457.

41. Corvera, E., O. Mouritsen, M. Singer, and M. Zuckermann. 1992. The permeability and the effect of acyl-chain length for phospholipid bilayers containing cholesterol: theory and experiment. *Biochim. Biophys. Acta*. 1107:261–270.

42. Warschawski, D. E., and P. F. Devaux. 2005. Order parameters of unsaturated phospholipids in membranes and the effect of cholesterol: a ^{1}H-^{13}C solid-state NMR study at natural abundance. *Eur. Biophys. J*. 34: 987–996.

43. de Almeida, R. F., A. Fedorov, and M. Prieto. 2003. Sphingomyelin/phosphatidylcholine/cholesterol phase diagram: boundaries and composition of lipid rafts. *Biophys. J*. 85:2406–2416.

44. Galla, H. J., and W. Hartmann. 1980. Excimer-forming lipids in membrane research. *Chem. Phys. Lipids*. 27:199–219.

45. Pansu, R. B., K. Yoshihara, T. Arai, and K. Tokumaru. 1952. 1993. Convolution analysis of the pyrene excimer formation in membranes. *J. Phys. Chem.* 97:1125–1133.

46. Kahya, N., and P. Schwille. 2006. How phospholipid-cholesterol interactions modulate lipid lateral diffusion, as revealed by fluorescence correlation spectroscopy. *J. Fluoresc*. 16:671–678.

47. Chu, P., S. Murray, D. Lissin, and M. von Zastrow. 1997. Delta and kappa opioid receptors are differentially regulated by dynamin-dependent endocytosis when activated by the same alkaloid agonist. *J. Biol. Chem.* 272:27124–27130.

48. Salamon, Z., S. Cowell, E. Varga, H. I. Yamamura, V. J. Hruby, and G. Tollin. 2000. Plasmon resonance studies of agonist/antagonist binding to the human δ-opioid receptor: new structural insights into receptor-ligand interactions. *Biophys. J*. 79:2463–2474.

49. Epand, R. M. 2004. Do proteins facilitate the formation of cholesterol-rich domains? *Biochim. Biophys. Acta*. 1666:227–238.

50. Dumas, F., J. F. Tocanne, G. Leblanc, and M. C. Lebrun. 2000. Consequences of hydrophobic mismatch between lipids and melibiose permease on melibiose transport. *Biochemistry*. 39:4846–4854.

51. Dumas, F., M. C. Lebrun, and J. F. Tocanne. 1999. Is the protein/lipid hydrophobic matching principle relevant to membrane organization and functions? *FEBS Lett*. 458:271–277.

52. Marie, N., I. Lecoq, P. Jauzac, and S. Allouche. 2003. Differential sorting of human δ-opioid receptors after internalization by peptide and alkaloid agonists. *J. Biol. Chem*. 278:22795–22804. *Epub*. 22003: 22792.

53. Lopez, A., and C. Le Roux. 2006. Characterization of the lipid membrane state of living cells using a pyrene probe mimicking the cholesterol: application to protein screening. International reference: WO2006/100388 A2; Patent France No. 05/02884.